Article

Dynamical Change of Signal Complexity in the Brain During Inhibitory Control Processes

Shih-Lin Huang [1,2], Philip Tseng [3] and Wei-Kuang Liang [1,*]

[1] Institute of Cognitive Neuroscience, National Central University, Jhongli 32001, Taiwan;
    E-Mail: huang.shih.lin@gmail.com
[2] Department of Physics, National Central University, Jhongli 32001, Taiwan
[3] Graduate Institute of Humanities in Medicine, Taipei Medicine University, Taipei 11031, Taiwan;
    E-Mail: philip@tmu.edu.tw

* Author to whom correspondence should be addressed; E-Mail: wkliang@cc.ncu.edu.tw;
    Tel.: +886-3-4227151 (ext. 65212); Fax: +886-3-4263502.

Abstract: The ability to inhibit impulses and withdraw certain responses are essential for human's survival in a fast-changing environment. These processes happen fast, in a complex manner, and require our brain to make a fast adaptation to inhibit the impulsive response. The present study employs multiscale entropy (MSE) to analyzing electroencephalography (EEG) signals acquired alongside a behavioral stop-signal task to theoretically quantify the complexity (indicating adaptability and efficiency) of neural systems to investigate the dynamical change of complexity in the brain during the processes of inhibitory control. We found that the complexity of EEG signals was higher for successful than unsuccessful inhibition in the stage of peri-stimulus, but not in the pre-stimulus time window. In addition, we found that the dynamical change in the brain from pre-stimulus to peri-stimulus stage for inhibitory control is a process of decreasing complexity. We demonstrated both by sensor-level and source-level MSE that the processes of losing complexity is temporally slower and spatially restricted for successful inhibition, and is temporally quicker and spatially extensive for unsuccessful inhibition.

Keywords: multiscale entropy; MSE; inhibitory control; stop signal; EEG; complexity; adaptability

1. Introduction

Cognitive control refers to brain functions that allow information processing and behavior to vary adaptively from moment to moment depending on our current goals, rather than remaining rigid and inflexible (e.g., [1]). Among these cognitive functions, inhibitory control reflects the ability to suppress a prepotent response and requires our brain to make a fast adaptation to inhibit the response. For example, a driver must respond to the rapid onset of a yellow light by inhibiting and switching from gas to brake. In the laboratory, inhibitory control is often investigated using a stop-signal task [2,3], where a "go" signal requires a motor response from the participants, but an irregularly-intervening sudden "stop" signal requires the response to be inhibited (e.g., [4–6]). To understand the process of inhibitory control in the brain, prior research has acquired brain signals (e.g., BOLD signal, ECoG, and EEG) from essential loci/electrodes during the stop signal task, and introduced some promising physiological measures that are related to behavioral performance of inhibitory control (e.g., [7–9]). However, beyond merely demonstrating a relationship between certain physiological measures and the behavioral performance, there is a need to investigate these brain signals using a measure that is able to theoretically quantify the adaptability and complexity of neural systems during the processes of inhibitory control.

To better investigate the adaptability and complexity of the neural systems during the stop-signal task, a 2014 study by Liang *et al.* [10] calculated the multiscale entropy (MSE; [11–14]) of EEG signals acquired along with the stop-signal experiment. The prior study was based on three hypotheses: (1) the complexity of a biological system reflects its ability to adapt and function in a fast-changing environment; (2) biological systems need to operate across multiple spatial and temporal scales, and hence their complexity is also multi-scaled; (3) the "ability to adapt" by the brain for a cognitive function is associated with the neuroplasticity of this function [10,14,15]. However, the prior study only applied MSE to EEG signals approximately from the go signal onset to the end of the stop-signal reaction time (SSRT). The aim of the current study is to reveal the dynamical change of complexity in the brain by applying MSE not only to the brain signals acquired during the stage of peri-stimulus, but also prior to stimulus onset during the stage of pre-stimulus. We hypothesize that these dynamical changes of complexity in the brain are related to whether the current attempt on response in the stop-signal task can be successfully inhibited or not. In addition, to further understand the sources of these dynamical changes of complexity, we employed an algorithm of beamformer spatial projection to calculate MSE at the source level.

2. Materials and Methods

Eighteen neurologically normal adults (10 males, mean age = 25.4) participated in the experiment. Informed consent was obtained from each participant before the experiment. The experiment was approved by the Institutional Review Board of the Chang-Gung Memorial Hospital (Taoyuan, Taiwan).

2.1. Stop-Signal Paradigm

The stop-signal task consisted of two types of trials: go, which was signaled with an arrow, and stop, which was signaled with an arrow followed by a diamond (Figure 1). In a go trial, each session began with a 500 ms central fixation cross, followed by a 200 ms blank screen. After the blank screen, an arrow

(go signal) pointing either to the right or left was displayed, and participants were told to respond to the direction of the arrow with their corresponding index finger as soon as possible. Participants were also told that sometimes the arrow would be followed by a diamond (stop-signal) in the center of the display after a delay (stop-signal delay (SSD)), and that they should withhold their responses if the diamond appeared.
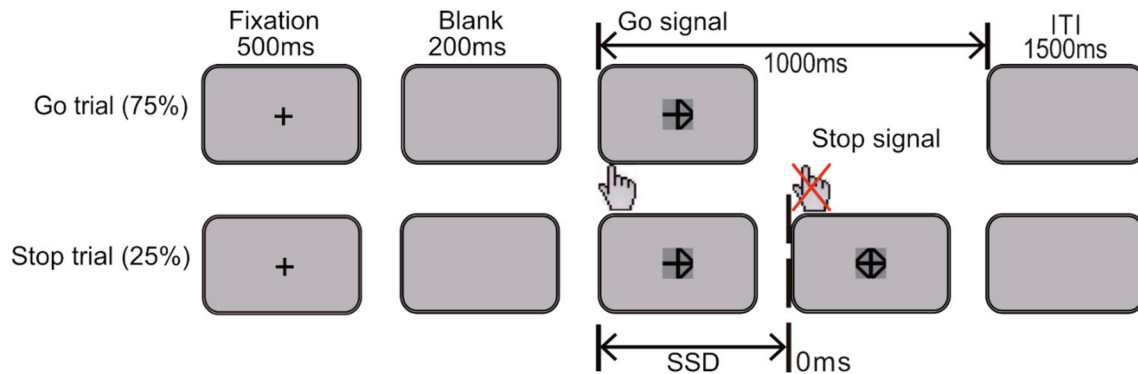

Figure 1. Illustration of the stop-signal task. ITI: inter-trial interval.

In the beginning of this experiment, participants were also given two preliminary blocks before the formal experimental session in order to determine their choice reaction time (CRT) and critical SSD. To determine each participant's CRT, the first preliminary block consisted of 80 go trials, and the individual-specific mean CRT and standard deviation from this block were used to monitor participants' performance in the subsequent block and formal session. Thus, the first block gave each participant an individually tailored timeframe for the go signal for the following sessions so that the timeframe was neither too easy nor too difficult. If a participant's CRT on any trial in any of the subsequent sessions was two standard deviations longer than their mean CRT from this block, they would receive visual feedback saying "You did not press the button fast enough" to serve as a reminder to press the button as soon as the arrow appeared. This procedure has been demonstrated to effectively limit the strategy of intentionally slow responses that participants sometimes use to avoid errors ([16–18]).

In the second preliminary block, 90 go trials and 30 stop trials were presented. The initial SSD was set at 200 ms, and gradually moved lower or higher as the algorithm tracked the participant's success rate. If the participant's response in a stop trial was correct, the level of difficulty of the next stop trial would be increased by adding 50 ms to the SSD. If the participant's response was incorrect, the SSD in the next stop trial would be reduced by 50 ms. At the end of this block, a critical SSD for each participant was obtained via this tracking method, which gives an overall inhibition probability of approximately 50% in every individual.

Finally, the formal experimental session was conducted in three identical blocks, each lasting approximately 7 min. This was done so that participants could have a short break at around the same time interval. In each of these blocks, three types of SSDs were used: 50 ms less than the critical SSD (SSD1; an easier condition), critical SSD (*i.e.*, SSD2), and 50 ms more than the critical SSD (SSD3, a harder condition). 30 stop trials (10 trials for each type of SSD) were randomly interleaved with 90 go trials within each block, resulting in a total of 120 trials per block (*i.e.*, a total of 360 trials in all three blocks). This randomized and interleaved design was used here because it minimizes the possibility of participants' different speeds for each type of trial.

2.2. EEG Recording and Preprocessing

EEG was continuously recorded with 62 Ag/AgCl electrodes mounted on a plastic cap (SynAmps2, NeuroScan, Victo-ria, Australia). The sampling rate was 1000 Hz, with an analog 0.05–70 Hz bandpass filter. The reference was placed between channel Cz and CPz and the ground electrode was placed between FPz and Fz. Additionally, two sets of bi-polar electrodes were placed on the upper and lower side of the left eye and on the canthi of both eyes to measure vertical (VEOG) and horizontal (HEOG) eye-movements. Impedances of all electrodes were below 5 kΩ.

A correction for eye-blinks was first applied to the EEG data acquired, with eye-blink peaks derived from VEOG by means of regression and correlation. All channels were re-referenced off-line to the average of the two mastoids (M1 and M2). The onset of the stop-signal was set as the zero point, and epochs ran from −900 to 900 ms. Artifact rejection was performed to exclude trials with EEG amplitude > ±150 μV, and EOG amplitude > ±50 μV.

2.3. MSE Analysis

Brain signal complexity in different scales was estimated using multiscale entropy analysis (MSE). Before performing MSE, we employed empirical mode decomposition (EMD) [19] to remove trend (last component of EMD) from the epoched EEG data. This detrend process by EMD has been demonstrated as efficient to improve the stationarity of the signals [20–23]. For stop trials, the MSE analysis was performed from scale 1 to 30 (the resolution of EEG signals is 1 ms) in two time windows: (1) −750~−300 ms; and (2) −300~150 ms relative to the stop signal onset. Since the first window was generally before the go signal onset, and the second window was between the go signal onset and prior to the end of SSRT, in the following we simply refer the two windows as the *pre-stimulus* and *peri-stimulus* stage, respectively. In addition, to demonstrate that a decrease in complexity is necessary for motor response, MSE for go trials was also analyzed both in the "prior-go" (from 450 ms prior to go signal to the go signal onset) and "post-go" (from the go signal onset to 450 ms after the go signal) time windows. The MSE was calculated in two steps. First, the algorithm progressively down-samples the EEG time series $\{x_1, \ldots, x_i, \ldots, x_N\}$ for each stage of each trial in each condition. This down-sampling procedure was defined as a coarse-grained procedure along various scales in MSE analysis. For timescale τ, the coarse-grained time series $Y^{(\tau)} = \{y(1), y(2), \ldots, y(\tilde{N}^{(\tau)})\}$ is obtained by averaging data points within non-overlapping windows of length τ. Therefore each element of a coarse-grained time series, j, is calculated according to:

$$y(j) = \frac{1}{\tau}\sum_{i=(j-1)\tau+1}^{j\tau} x_i, \text{ where } 1 \le j \le \tilde{N}^{(\tau)}, \tilde{N}^{(\tau)} = \frac{N}{\tau} \tag{1}$$

Second, the algorithm computes the sample entropy for each coarse-grained time series $Y^{(\tau)}$. Note that all the superscripts (τ) are omitted in the following to simplify the notations. There are two specified parameter for calculating the sample entropy: pattern length m and tolerance level r for similarity comparison. Given the coarse-grained time series Y, sample entropy is calculated as follows: first, construct $\tilde{N} - m + 1$ vectors:

$$Y_m(i): Y_m(i) = \{y(i+k)\}, 0 \le k \le m-1 \tag{2}$$

and the distance between two vectors is defined as absolute maximum difference between the corresponding scalar components:

$$d[Y_m(i), Y_m(j)] = \max(|y(i+k) - y(j+k)|), 0 \le k \le m-1 \tag{3}$$

Given r, $n_i'^m$ is defined as the number of vectors $Y_m(j)$ falling within vector distance $r*s$ of $Y_m(i)$ without allowing self-matches, where s is the standard deviation of the original time series. Similarly, $n_i'^{m+1}$ is defined as the number of vectors $Y_{m+1}(j)$ falling within vector distance $r*s$ of $Y_{m+1}(i)$. Finally, Sample entropy is defined by the negative natural logarithm of the conditional probability that a time series of length $\tilde{N}$, having repeated itself within a tolerance $r*s$ (similarity factor) for m points pattern, will also repeat itself for $m + 1$ points pattern:

$$S_E(m, r, \tilde{N}) = \ln \frac{\sum_{i=1}^{\tilde{N}-m} n_i'^m}{\sum_{i=1}^{\tilde{N}-m} n_i'^{m+1}} \tag{4}$$

Although there are no recommendations in terms of the best values for parameters for calculating sample entropy values in EEG studies, some theoretical and clinical applications have suggested setting $m = 1$ or 2 and $r = 0.1$ to 0.3 to provide a high validity for sample entropy in EEG signals (e.g., [24–26]). In the present study the pattern length, m, was set to 1; that is, one data point was used for pattern matching; the similarity criterion, r, was set to 0.3, meaning that data points were considered to be indistinguishable if the absolute amplitude difference between them was $\le 30\%$ of the time series standard deviation. Because previous research has suggested that data lengths of 10^m to 20^m (m: pattern length) should be sufficient to estimate sample entropy [27], the length of data in both stages (450 time points before coarse-graining procedure) may be sufficient for $m = 1$ with scales 1~30. EEG data processing was performed using SPM8 and custom MATLAB (Math Works, Natick, MA, USA) scripts. The MSE analysis algorithm can be found at http://www.physionet.org/physiotools/mse/.

2.4. Source Level MSE

To obtain MSE in source space, a virtual electrode approach applying linearly constrained minimum variance (LCMV) spatial filtering Beamformer [28] to the detrended sensor-level data from each stage (please see Sections 2.2 and 2.3) was used. To obtain the leadfields (physical forward model) for the LCMV Beamformer, a boundary element head model was constructed from an MNI template brain (Colin 27). The sensor-level data were projected into source space by multiplying it with the spatial accordant filters, resulting in source-level data of 1963 virtual electrodes with a spacing of 1 cm inside the volume of cortex. MSE was calculated for data from each of the virtual electrodes, and the parameters of MSE were the same as the sensor-level MSE analysis, as indicated in Section 2.3.

After applying MSE to the source-level data, source statistics (see next section) were computed and resulted in a mask of significance, as well as a t map. The resulting t map was subsequently projected and interpolated to a cortical mesh of the same MNI template brain for illustrative purposes.

The Beamformer projection was performed using FieldTrip toolbox (http://www.fieldtriptoolbox.org/) [29] and custom MATLAB (Math Works) scripts.

2.5. Statistical Method

A cluster-based non-parametric permutation (CBnPP) test [30,31] was employed to test the differences of MSE between each pair of conditions for both the sensor and source level data. Originally, this method was used to provide weak family-wise error rate (FWER) control for EEG- and MEG-data by grouping test results at nearby sensors and time points into clusters based on their statistical significance and proximity. The current employment of this method is by grouping the test results of MSE at nearby sensors/sources and scales into clusters. In this study, two sensors/sources were identified as neighbors if the distance between both was less than 50 mm/10 mm, and 2000 permutations were performed for each test. This method has the advantage of protecting the multiple comparison errors, yet it is powerful (less conservative, in comparison with the Bonferroni or false discovery rate correction) to reveal significant effects, especially for the clustered effect like that from EEG data, as well as the MSE results of EEG signals.

3. Results

Behavioral results are shown in Table 1, where non-cancelled rate is the rate of stop trials in which the responses were not successfully inhibited after the stop signal onset, and SSRT is the stop-signal reaction time which was modeled as a race between the stop and go processes to obtain a measure for estimating the time needed to inhibit a response [2]. For the following MSE analysis, we further divided these stop trials into successful-stop (SST) and unsuccessful-stop (USST) trials.

Table 1. Behavior data in inhibitory control.

Accuracy of go trials	97.90% (0.36%)
Mean RT of go trials (ms)	383.59 (5.72)
Mean RT of USST (ms)	362.77 (5.82)
SSRT (ms)	202.41 (3.85)
Mean SSD (ms)	188.56 (9.08)
Non-cancelled rate (SSD1)	21.02% (2.72%)
Non-cancelled rate (SSD2)	55.93% (3.34%)
Non-cancelled rate (SSD3)	85.93% (2.90%)

Note: Standard errors are showed in brackets.

3.1. Analysis of Variance for MSE

The 62-channel EEG signals, acquired along with the stop-signal experiment, were analyzed by the MSE algorithm from scale 1 to 30. To reveal all the pattern differences of MSE in the experiment, repeated measures three-way analyses of variance (ANOVAs) that included the factors of "Inhibition" (successful- *vs.* unsuccessful-stop), "Scale Range" (SR) (small-scale: 1–10, medium-scale: 11–20, and large-scale: 21–30; obtained by averaging the MSE across scales within each of the three scale range), and "Stage" (pre-stimulus *vs.* peri-stimulus) as three within-subject factors were conducted on the MSE of brain signals from each EEG channel (Figure 2; each EEG channel enclosed by a dark green circle indicated that the main effect or interaction on this channel was significant with false discovery rate (FDR) [32] control over all EEG channels at level less than 0.05). The results showed significant main

effects of "Stage" on EEG channels from middle and superior frontal to parietal brain regions, significant main effects of "SR" over all EEG channels, and relatively sparse main effects of "Inhibition" over a few channels. These results indicated that the magnitude of MSE differed between the pre-stimulus and peri-stimulus stage, and varied among scale ranges. The ANOVAs also revealed significant first order "Inhibition-by-SR" interactions over EEG channels from frontal to parietal brain areas, "Inhibition-by-Stage" interactions on several EEG channels over superior frontal and parietal brain region, and "SR-by-Stage" interactions mainly over parietal region. The interactions "Inhibition-by-Stage" and "Inhibition-by-SR" indicated that the differences of MSE pattern between SST and USST trials may be more dominant in a specific stage, and in one or two scale ranges. Significant second order interactions (Inhibition*SR*Stage) were also found, but relatively sparse as compared to the first order interactions. On the basis of the first and second order interactions, we performed a repeated measures two-way ANOVA to see the simple "Inhibition-by-Stage" interactions and simple "Inhibition" and "Stage" main effects in each of the scale ranges. Figure 3 showed the simple ANOVA results. The significant simple main effects of "Stage" in small and medium scale range indicated that the differences of MSE between the pre-stimulus and peri-stimulus stage mainly stemmed from the small and medium scales. The significant simple "Inhibition-by-Stage" interactions over frontal, parietal and occipital regions suggested that the dynamical changes of MSE from the pre-stimulus to peri-stimulus stage are different between SST and USST trials.
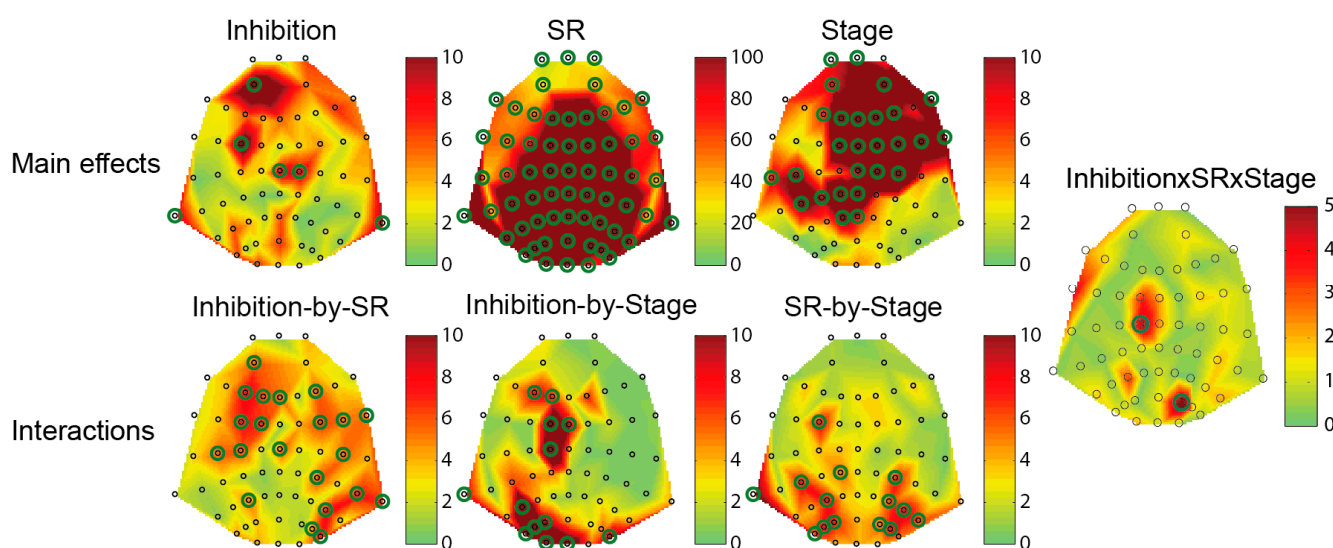

Figure 2. Main effects and interactions of the repeated measures 3-way ANOVAs with "Inhibition" (successful- *vs.* unsuccessful-stop), "Scale Range (SR)" (three ranges: small, medium, and large scale ranges), and "Stage" (pre-stimulus *vs.* peri-stimulus) as three within-subject factors. EEG channels enclosed by a dark green circle indicated that the main effect or interaction on this channel was significant ($p < 0.05$, FDR corrected). Color shades denoted *F* values.
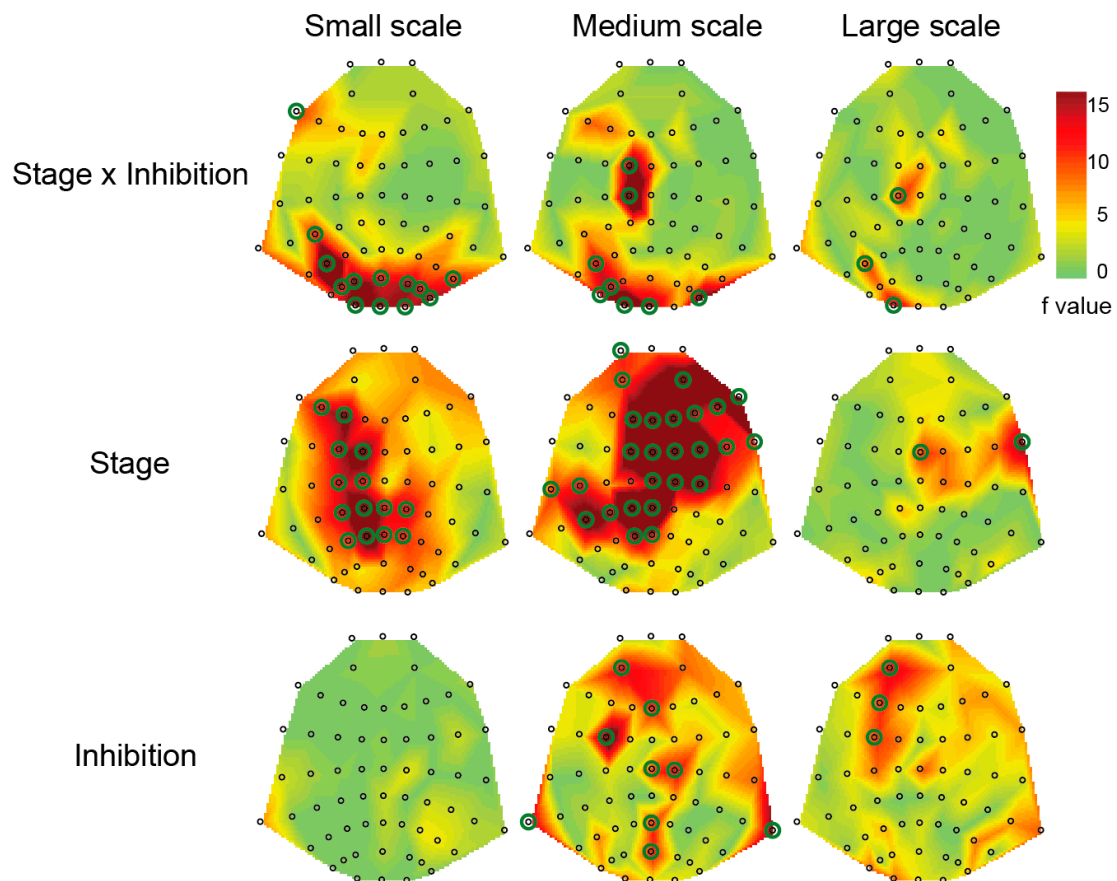
Figure 3. Main effects and interactions of the repeated measures 2-way ANOVAs for each scale range, with "Inhibition" (successful- *vs.* unsuccessful-stop), and "Stage" (pre-stimulus *vs.* peri-stimulus) as two within-subject factors. EEG channels enclosed by a dark green circle indicated that the main effect or interaction on this channel was significant ($p < 0.05$, FDR corrected). Color shades denoted *F* values.

For illustrative purposes, changes of MSE in small, medium, and large scales from the pre-stimulus to peri-stimulus stage of both SST and USST trials are shown in Figure 4 (ten representative EEG channels). There was a trend of decreasing MSE from the pre-stimulus to peri-stimulus stage, especially in USST trials. The MSE of SST trials was in general higher than that of USST trials, primarily in the peri-stimulus stage. Statistical results and explanations for these trends are provided below.

3.2. Sensor-Level MSE Contrasts (SST vs. USST; Pre-Stimulus vs. Peri-Stimulus)

Instead of using traditional post-hoc tests, the CBnPP test was employed both to further elucidate the pattern differences of MSE between each pair of conditions following the inferences from the ANOVAs, and to reveal clustered effects along the entire channels × scales space. We tested for difference in MSE between SST and USST trials, and these contrasts (as *t* values), both during the peri-stimulus and pre-stimulus stage, are shown in Figure 5a,b, respectively.
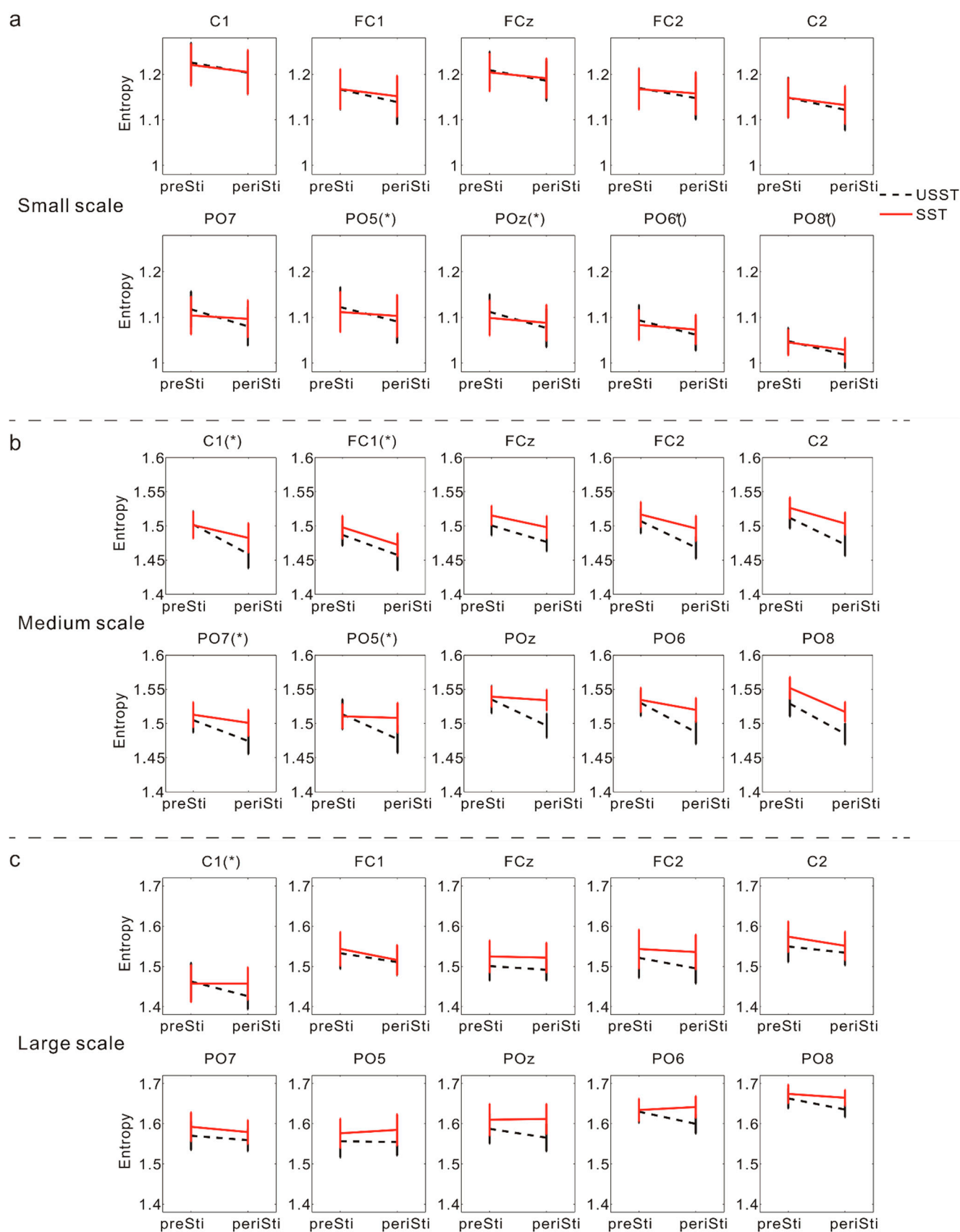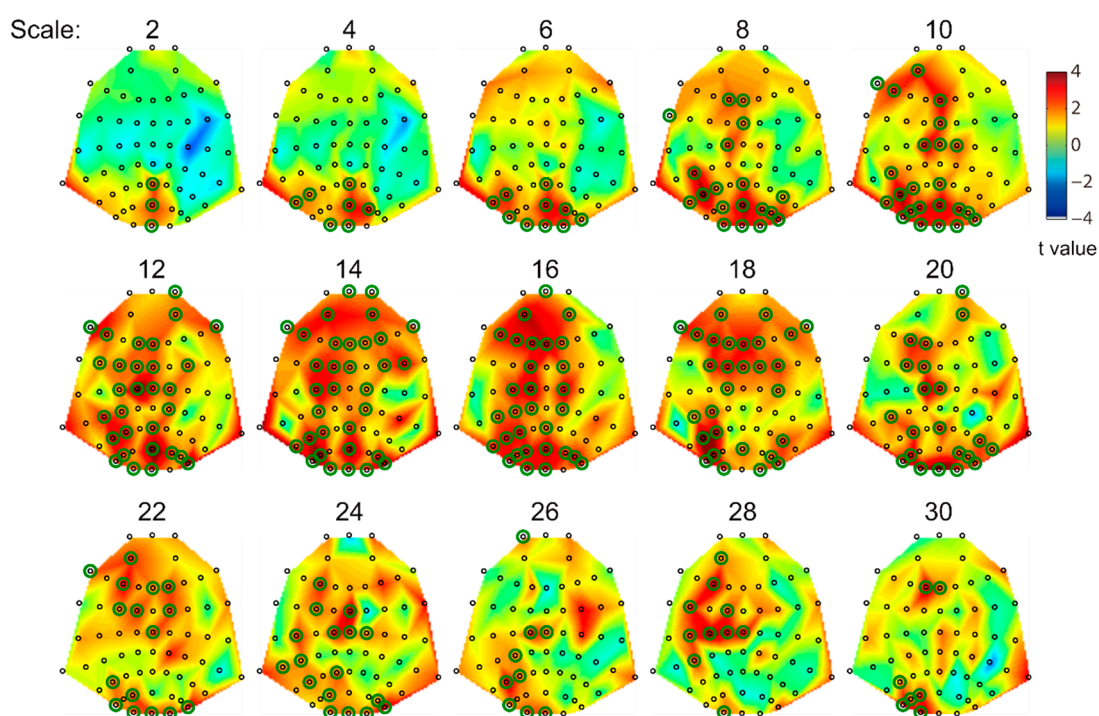
Figure 4. Change of MSE in (**a**) small, (**b**) medium, and (**c**) large scales from the pre-stimulus (preSti) to peri-stimulus (periSti) stage of both SST and USST trials. S.E.M. at each stage is indicated by the error bar.
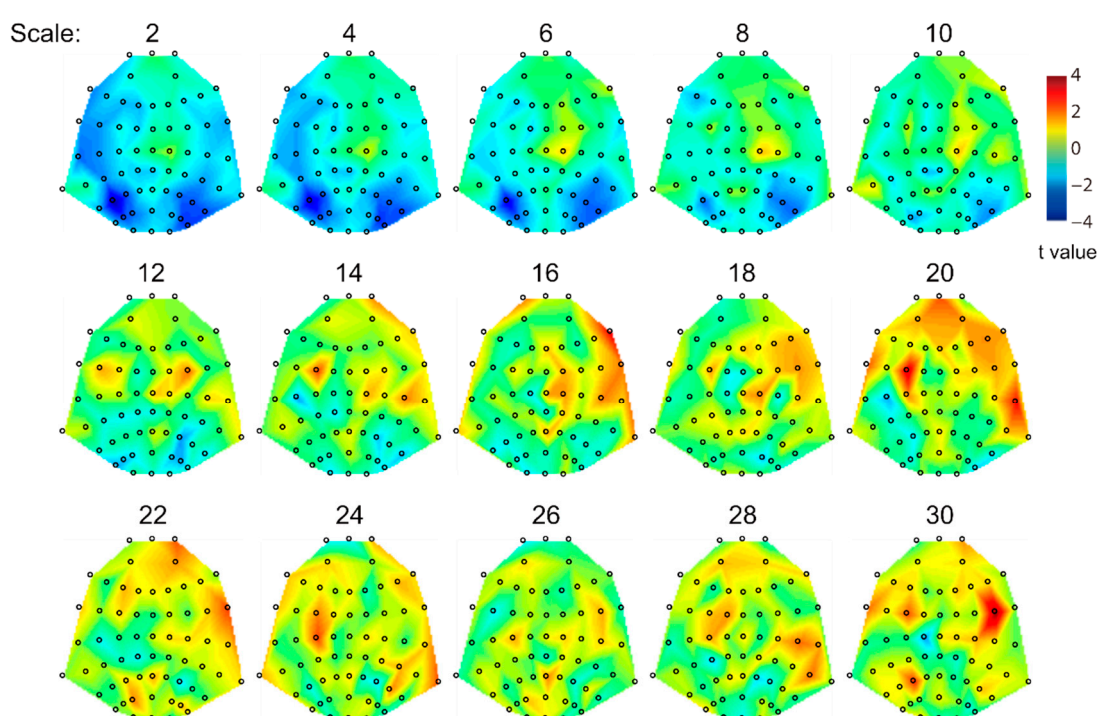
Figure 5. Contrast of MSE between SST and USST trials during the stage of (**a**) peri-stimulus, and (**b**) pre-stimulus, respectively. For each scale, the EEG channels enclosed by dark green circles denoted that the difference of sample entropy between SST and USST trials on these channels were significant ($p < 0.05$, $n = 18$, two tailed CBnPP test). Color shades denoted *T* values.

For each scale, the EEG channels enclosed by dark green circles denote that on each of these channels the difference of sample entropy between SST and USST trials was significant ($p < 0.05$, $n = 18$, two tailed CBnPP test). The results showed that the MSE was higher for SST as compared to USST trials in the peri-stimulus stage, but this effect of higher MSE in SST trials could not be observed in the pre-stimulus stage. Note that although we only showed the even scales (*i.e.*, 2, 4, …, 30) to save space in the following figures, the CBnPP test was performed along all scales. This simplification is plausible because the effects from the odd scales were approximately in between their two adjacent even scales when the resolution is 1 ms.

Furthermore, to demonstrate the decrease of MSE from the pre-stimulus to peri-stimulus stage, we tested for difference in MSE between the peri-stimulus and pre-stimulus stage, both for SST and USST trials. Within SST trials, the results showed that the MSE from scale 2 to 20 in the peri-stimulus stage is significantly lower as compared to the pre-stimulus stage ($p < 0.05$, $n = 18$, two tailed CBnPP test) (Figure 6a) on several EEG channels over frontal and parietal brain regions. For USST trials, the effect of MSE decrement from the pre-stimulus to peri-stimulus stage was even more steeper than that for SST trials (revealed by exceedingly negative t values in Figure 6b), and this effect extended to almost entire parietal and occipital EEG channels.

In addition, to demonstrate that a decrease in complexity is a necessary feature of motor actions, for go trials we also tested whether the MSE of "post-go" duration is lower than "prior-go" duration. The t contrast shown in Figure 6c indicated that the effect of MSE decrement from the prior-go to post-go stage was significant ($p < 0.05$, $n = 18$, two tailed CBnPP test). This robust effect signified that a decrease in complexity is indeed an essential signature of motor response.
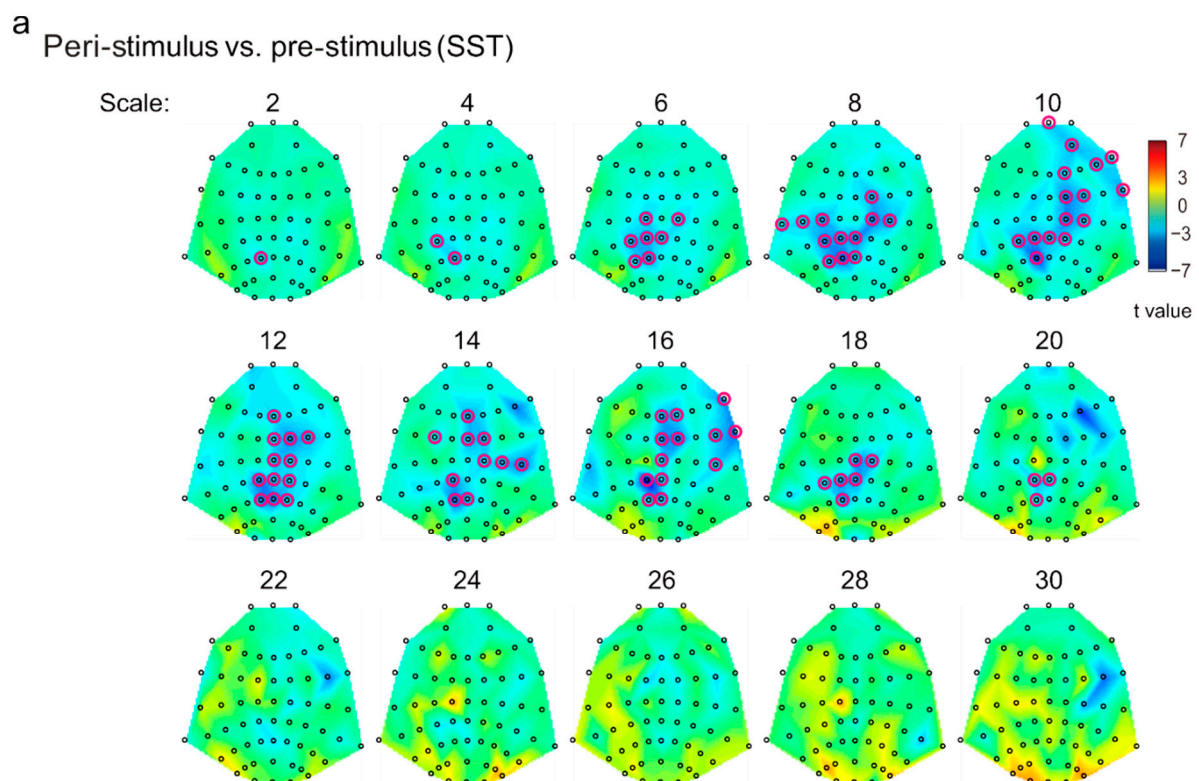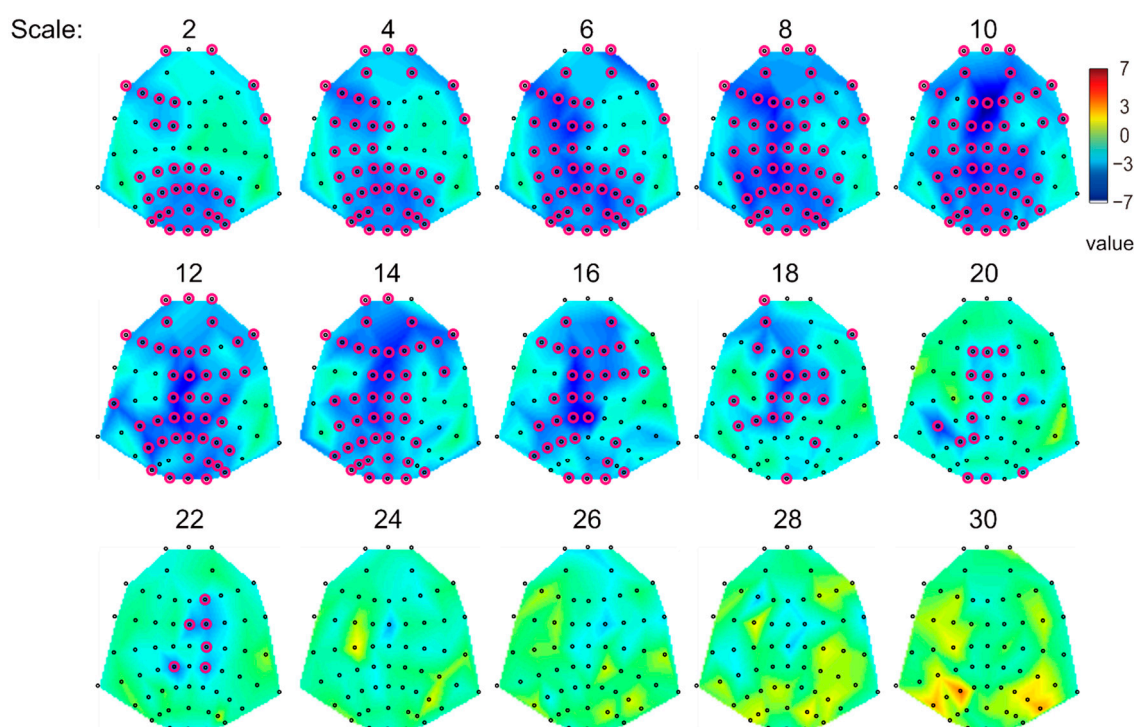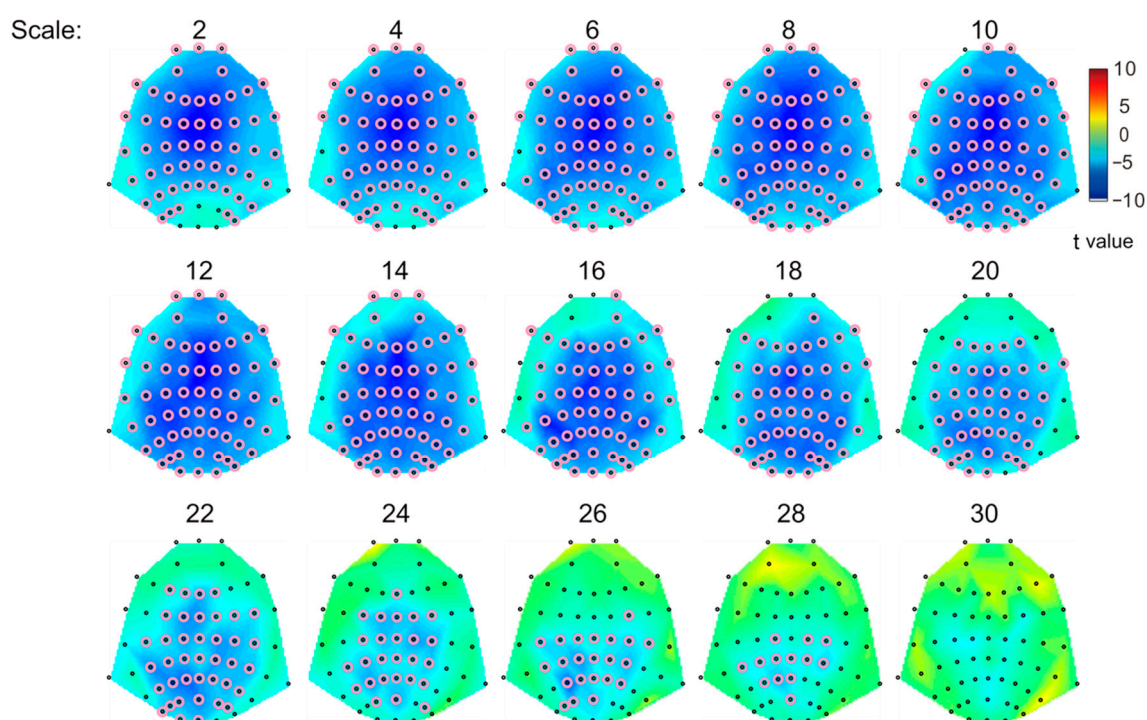

Figure 6. *Cont.*

Figure 6. Contrast of MSE between "peri-stimulus" and "pre-stimulus" stage for (**a**) successful, and (**b**) unsuccessful stop trials, respectively. (**c**) The contrast of MSE between "post-go" and "prior-go" for go trials. For each scale, the EEG channels enclosed by red circles denoted that the difference of sample entropy between the two stages on these channels were significant ($p < 0.05$, $n = 18$, two tailed CBnPP test). Color shades denoted T values.

3.3. Source-Level MSE Contrasts (SST vs. USST; Pre-Stimulus vs. Peri-Stimulus)

To better understand the source of these dynamical changes of MSE, we employed an algorithm of beamformer spatial projection to calculate MSE at the source level. Similar to the above sensor-level analysis, we employed the CBnPP test to reveal the pattern differences of source-level MSE between each pair of conditions. However, the current employment of CBnPP was along the virtual-sensors × scales space. Figure 7 shows the source-level MSE contrast between SST and USST trials during the peri-stimulus and pre-stimulus stage.
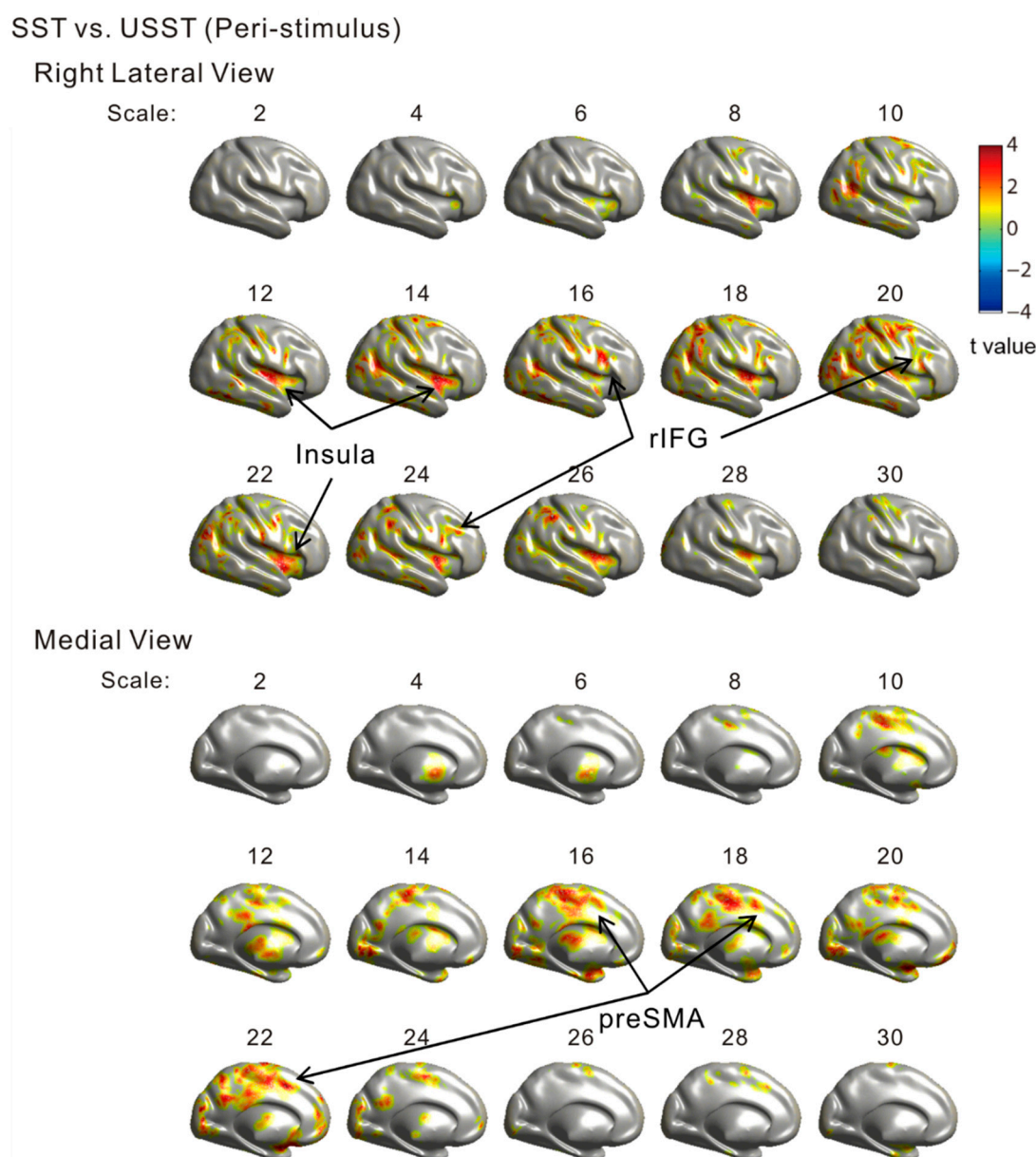

Figure 7. Source-level MSE contrast between SST and USST trials during the stage of peri-stimulus. Brain regions shown with colors (except gray, color shades denoted *t* values) indicated that the difference of sample entropy between SST and USST trials in these regions was significant ($p < 0.05$, $n = 18$, two tailed CBnPP test). The contrast was masked by the statistical results (gray color indicates that in this region the contrast was not significant, and therefore the corresponding *t* values were not shown).

In Figure 7 the contrast was shown by both the right lateral and left medial views to illustrate the brain areas in which the source-level MSE was significantly higher for SST *vs.* USST trials in the peri-stimulus stage ($p < 0.05$, $n = 18$, two tailed CBnPP test). These significant brain areas included some inhibitory control related areas (e.g., insula, right inferior frontal gyrus (rIFG), presupplementary motor area (preSMA)) identified by prior research (e.g., [4–6,30]), as well as some other areas over parietal and occipital lobes. No significant difference was found at the source-level MSE between SST and USST trials in the pre-stimulus stage, consistent with the corresponding sensor-level results. Moreover, we tested the difference of source-level MSE between the peri-stimulus and pre-stimulus stage both for SST and USST trials. For SST trials, inconsistent with the sensor-level result, the contrast showed no difference between the peri-stimulus and pre-stimulus stage under the CBnPP test. To demonstrate that there was still a trend of decreasing MSE for SST trials, instead of using the CBnPP test, we masked the contrast with a less conservative statistics ($p < 0.01$, two-tailed *t*-tests, uncorrected), as shown in Figure 8.
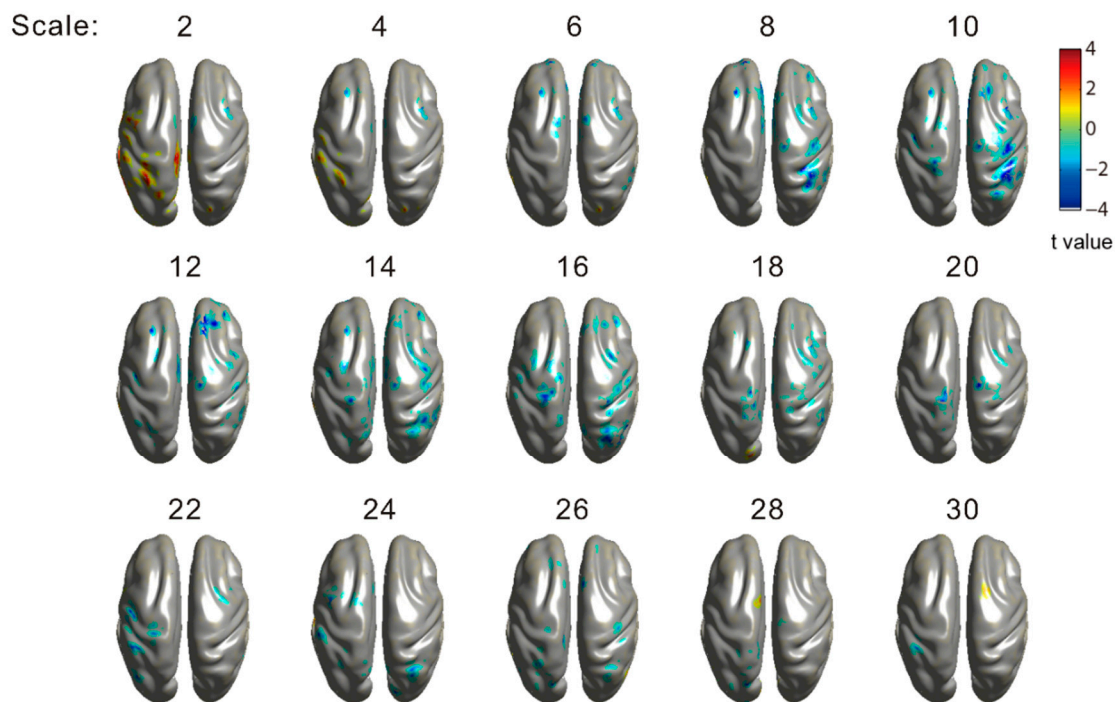

Figure 8. Source-level MSE contrast between "peri-stimulus" and "pre-stimulus" stage for successful stop trials. This contrast was masked by a less conservative statistics ($p < 0.01$, two-tailed *t*-tests, uncorrected) to show the trend of decreasing complexity in the brain.

This less conservative result for SST trials showed that the areas of lower MSE for the peri-stimulus *vs.* pre-stimulus stage were restricted. Conversely, for USST trials, significantlower source-level MSE for the peri-stimulus as compared to pre-stimulus stage was found by the CBnPP test ($p < 0.05$, $n = 18$, two tailed), which was consistent with the corresponding sensor-level counterpart and was shown in Figure 9. This result for USST trials showed multiple broad areas of lower MSE for the peri-stimulus in comparison to the pre-stimulus stage. The inconsistency between the source-level and sensor-level result in SST trials could be caused by the strategy of protecting multiple comparison errors in the CBnPP test

(*i.e.*, too many comparisons were involved in the source-level analysis). However, this inconsistency may also indicate that the decreasing of MSE in SST trials was limited and not as robust as that in USST trials.
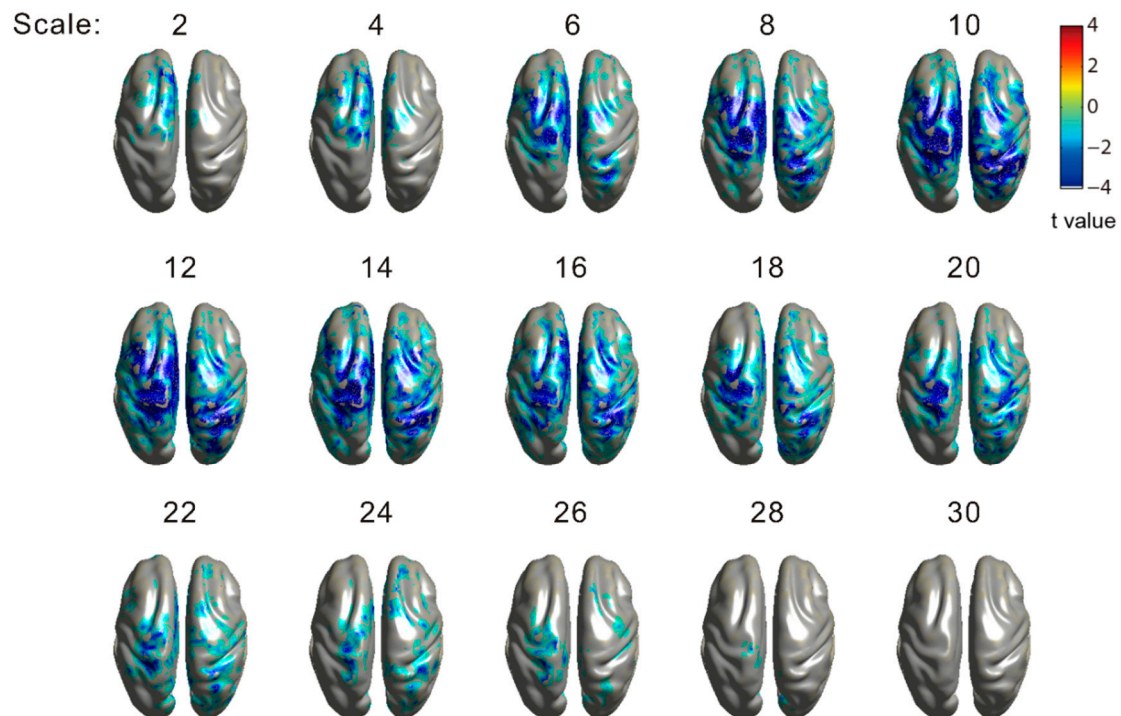

Figure 9. Source-level MSE contrast between "peri-stimulus" and "pre-stimulus" stage for unsuccessful stop trials. Brain regions shown with colors (except gray) denoted that the difference of sample entropy between peri-stimulus and pre-stimulus stage in these regions were significant ($p < 0.05$, $n = 18$, two tailed CBnPP test). Convention is the same as Figure 7.

4. Discussion

4.1. The MSE Perspective

The present study employed the MSE analysis to theoretically quantify and reveal the dynamical change of complexity in the brain from the stage of pre-stimulus to the stage of peri-stimulus for inhibitory control. We found that (1) the complexity of EEG signals was higher for successful than unsuccessful inhibition in the stage of peri-stimulus, and this effect was not significant in the stage of pre-stimulus; and (2) the dynamical change in the brain from the stage of pre-stimulus to the stage of peri-stimulus for inhibitory control was a process of decreasing MSE, and this effect was especially robust for unsuccessful inhibition. According to the above two findings, within the limits of the available database, we propose that (1) the cost of preparing a motor response is losing complexity in the brain; and (2) a successful-stop trial corresponds to a process of losing complexity that is temporally slower and spatially restricted, whereas an unsuccessful-stop trial can be seen as the result of a temporally quicker process of losing complexity, and this rapid complexity-losing process propagates over extensive brain areas.

Based on one hypothesis of MSE that the complexity of a biological system reflects its ability to adapt and function in a fast-changing environment, the process of losing complexity in this study implies losing adaptability when preparing a response in inhibitory control. From the contrast of MSE between the stage of peri-stimulus and the stage of pre-stimulus, both at the sensor and source levels, this trend of losing adaptability may propagate to extensive brain areas or just be limited to few brain areas. For any given trial if the trend of losing adaptability propagates to a number of widespread brain areas, it would be more likely to fail in inhibiting the response due to decreased adaptability among extensive neural systems. Conversely, for a trial that the trend of losing adaptability was restricted to only a small number of brain areas, because the adaptability of neural systems remained high, the possibility of successful inhibition also remains high.

4.2. Inference from Sensor-Level MSE

Both the three-way and two-way ANOVAs of sensor-level MSE in the present study indicated significant interactions between Inhibition (SST *vs.* USST) and Stage (pre-stimulus *vs.* peri-stimulus) in small and medium scales on EEG channels over parietal and occipital brain regions. Together with the MSE contrast between SST and USST trials at each stage, and the MSE contrast between the peri-stimulus and pre-stimulus stage for each trial type (SST|USST), all these results pointed to that losing complexity on EEG signals from the parietal and occipital brain regions were unfavorable to inhibitory control. Furthermore, for go trials, the MSE contrast indicated that the effect of MSE decrement from the prior-go to post-go stage is a critical feature for motor response. Because there should be no inhibitory process (at least not dominant) in these go trials, a decrease in complexity may be a general feature of engaging motor actions.

For the SST trials, because the decrease of complexity was not so dramatic, according to the aforementioned basic hypothesis of MSE, the adaptability of the neural systems remained high and thus successfully inhibited an initiated motor response.

4.3. Inference from Source-Level MSE

The results of source-level MSE in the present study indicated that sustained high complexity in inhibitory control is related to brain regions such as insula, rIFG, and preSMA, and such process is essential for successful inhibition (Figure 7). This implies that these brain areas are highly adaptable during the process of inhibitory control, *i.e.*, keeping high adaptability in insula, rIFG, and preSMA is important for a successful inhibitory control. Figure 7 also indicated that the scales where the complexity of SST is higher than USST in preSMA are approximately the same as that in rIFG. This result supports the idea that both preSMA and rIFG are involved in the same inhibitory network (e.g., [33,34]). In addition, the results also pointed to higher complexity for SST than USST trials in some brain regions such as the parietal and occipital lobes, but the scales where these effects were revealed are different from that in preSMA and rIFG. Although it is difficult to explain the individual role of each identified brain region based on the current findings, these brain regions inferred from the source-level MSE suggest that the brain network(s) for inhibitory control can be more extensive than that proposed by prior research [4–6].

The consistency between the present source-level and sensor-level MSE results suggest that the Beamformer spatial projection can faithfully preserve the complexity in the original brain signals. This suggests a novel direction for future MSE studies of EEG/MEG brain signals that not only pertains to performing sensor-level MSE analysis, but also conducting source-level MSE analysis.

4.4. Methodological Considerations

Recently, MSE has been extended for taking account the multivariate nature of EEG signal. The purpose of multivariate MSE is to reveal both the within and cross-channel dependencies in multichannel data [35–38]. Therefore, an alternative approach to demonstrate the results in the present study is to employ Multivariate Empirical Mode Decomposition (MEMD) [39] to detrend the EEG data, followed by using the multivariate MSE to quantify the complexity of the brain signals. This approach may improve the current results, and will be one of our future studies.

4.5. Conclusions

In summary, this study utilized MSE to characterize the dynamical change of complexity in EEG brain signals during inhibitory control, both at the sensor and source levels. More importantly, this study also suggests that the cost of an attempt to respond in inhibitory control is losing complexity in the brain. We demonstrated that in both sensor and source levels, the trend of losing complexity for successful inhibition was restricted, whereas this trend was much more significant for unsuccessful inhibition. According to the source-level MSE results, deficits of complexity in areas related to inhibitory control (e.g., insula, rIFG, and preSMA), as well as some areas over the parietal and occipital cortex, is unfavorable to the processes of inhibitory control.

Acknowledgments

Author Contributions

Shih-Lin Huang, Philip Tseng, and Wei-Kuang Liang conceived and designed the experiments. Shih-Lin Huang analyzed the data. Shih-Lin Huang and Wei-Kuang Liang wrote the paper. Philip Tseng participated in the discussion and checked the results. All authors have read and approved the final manuscript.

Conflicts of Interest

The authors declare no conflict of interest.

References

1. Solomon, M.; Yoon, J.H.; Ragland, J.D.; Niendam, T.A.; Lesh, T.A.; Fairbrother, W.; Carter, C.S. The development of the neural substrates of cognitive control in adolescents with autism spectrum disorders. *Biol. Psychiatry* **2013**, *76*, 412–421.

2. Logan, G.D.; Cowan, W.B. On the Ability to Inhibit Thought and Action—A Theory of an Act of Control. *Psychol. Rev.* **1984**, *91*, 295–327.

3. Logan, G.D.; Irwin, D.E. Don't look! Don't touch! Inhibitory control of eye and hand movements. *Psychon. Bull. Rev.* **2000**, *7*, 107–112.

4. Li, C.S.R.; Huang, C.; Constable, R.T.; Sinha, R. Imaging response inhibition in a stop-signal task: Neural correlates independent of signal monitoring and post-response processing. *J. Neurosci.* **2006**, *26*, 186–192.

5. Li, C.S.; Yan, P.; Sinha, R.; Lee, T.W. Subcortical processes of motor response inhibition during a stop signal task. *Neuroimage* **2008**, *41*, 1352–1363.

6. Swann, N.C.; Cai, W.; Conner, C.R.; Pieters, T.A.; Claffey, M.P.; George, J.S.; Aron, A.R.; Tandon, N. Roles for the pre-supplementary motor area and the right inferior frontal gyrus in stopping action: Electrophysiological responses and functional and structural connectivity. *NeuroImage* **2012**, *59*, 2860–2870.

7. Aron, A.R.; Poldrack, R.A. Cortical and subcortical contributions to stop signal response inhibition: Role of the subthalamic nucleus. *J. Neurosci.* **2006**, *26*, 2424–2433.

8. Swann, N.; Tandon, N.; Canolty, R.; Ellmore, T.M.; McEvoy, L.K.; Dreyer, S.; DiSano, M.; Aron, A.R. Intracranial EEG reveals a time- and frequency-specific role for the right inferior frontal gyrus and primary motor cortex in stopping initiated responses. *J. Neurosci.* **2009**, *29*, 12675–12685.

9. Lo, Y.H.; Liang, W.K.; Lee, H.W.; Wang, C.H.; Tzeng, O.J.; Hung, D.L.; Cheng, S.K.; Juan, C.H. The Neural Development of Response Inhibition in 5- and 6-Year-Old Preschoolers: An ERP and EEG Study. *Dev. Neuropsychol.* **2013**, *38*, 301–316.

10. Liang, W.K.; Lo, M.T.; Yang, A.C.; Peng, C.K.; Cheng, S.K.; Tseng, P.; Juan, C.H. Revealing the brain's adaptability and the transcranial direct current stimulation facilitating effect in inhibitory control by multiscale entropy. *NeuroImage* **2014**, *90*, 218–234.

11. Costa, M.; Goldberger, A.L.; Peng, C.K. Multiscale entropy analysis of complex physiologic time series. *Phys. Rev. Lett.* **2002**, *89*, 068102.

12. Costa, M.; Goldberger, A.L.; Peng, C.K. Multiscale entropy analysis of biological signals. *Phys. Rev. E* **2005**, *71*, 021906.

13. Peng, C.K.; Costa, M.; Goldberger, A.L. Adaptive Data Analysis of Complex Fluctuations in Physiologic Time Series. *Adv. Adapt. Data Anal.* **2009**, *1*, 61–70.

14. Goldberger, A.L.; Peng, C.K.; Lipsitz, L.A. What is physiologic complexity and how does it change with aging and disease? *Neurobiol. Aging* **2002**, *23*, 23–26.

15. Wang, C.H.; Tsai, C.L.; Tseng, P.; Yang, A.C.; Lo, M.T.; Peng, C.K.; Wang, H.Y.; Muggleton, N.G.; Juan, C.H.; Liang, W.K. The association of physical activity to neural adaptability during visuo-spatial processing in healthy elderly adults: A mulitscale entropy analysis. *Brain Cogn.* **2014**, *92*, 73–83.

16. Chen, C.Y.; Muggleton, N.G.; Tzeng, O.J.; Hung, D.L.; Juan, C.H. Control of prepotent responses by the superior medial frontal cortex. *Neuroimage* **2009**, *44*, 537–545.

17. Muggleton, N.G.; Chen, C.Y.; Tzeng, O.J.; Hung, D.L.; Juan, C.H. Inhibitory control and the frontal eye fields. *J. Cogn. Neurosci.* **2010**, *22*, 2804–2812.

18. Juan, C.H.; Muggleton, N.G. Brain stimulation and inhibitory control. *Brain Stimul.* **2012**, *5*, 63–69.

19. Huang, N.E.; Shen, Z.; Long, S.R.; Wu, M.C.; Shih, H.H.; Zheng, Q.; Yen, N.-C.; Tung, C.C.; Liu, H.H. The empirical mode decomposition and the Hilbert spectrum for nonlinear and non-stationary time series analysis. *Proc. R. Soc. Lond. Ser. A* **1998**, *454*, 903–995.

20. Costa, M.; Priplata, A.A.; Lipsitz, L.A.; Wu, Z.; Huang, N.E.; Goldberger, A.L.; Peng, C.K. Noise and poise: Enhancement of postural complexity in the elderly with a stochastic-resonance-based therapy. *Europhys. Lett.* **2007**, *77*, 68008.

21. Ho, Y.L.; Lin, C.; Lin, Y.H.; Lo, M.T. The prognostic value of non-linear analysis of heart rate variability in patients with congestive heart failure—A pilot study of multiscale entropy. *PLoS ONE* **2011**, *6*, e18699.

22. Park, C.; Kidmose, P.; Ungstrup, M.; Mandic, D.P. Time-Frequency Analysis of EEG Asymmetry using Bivariate Empirical Mode Decomposition. *IEEE Trans. Neural Syst. Rehabil. Eng.* **2011**, *19*, 366–373.

23. Labate, D.; Foresta, F.L.; Morabito, F.C.; Lay-Ekuakille, A.; Vergallo, P. Empirical mode decomposition *vs.* wavelet decomposition for the extraction of respiratory signal from single-channel ECG: A comparison. *IEEE Sens. J.* **2013**, *13*, 2666–2674.

24. Escudero, J.; Abasolo, D.; Hornero, R.; Espino, P.; Lopez, M. Analysis of electroencephalograms in Alzheimer's disease patients with multiscale entropy. *Physiol. Meas.* **2006**, *27*, 1091–1106.

25. Takahashi, T.; Cho, R.Y.; Mizuno, T.; Kikuchi, M.; Murata, T.; Takahashi, K.; Wada, Y. Antipsychotics reverse abnormal EEG complexity in drug-naive schizophrenia: A multiscale entropy analysis. *NeuroImage* **2009**, *51*, 173–182.

26. Yang, A.C.; Wang, S.J.; Lai, K.L.; Tsai, C.F.; Yang, C.H.; Hwang, J.P.; Lo, M.T.; Huang, N.E.; Peng, C.K.; Fuh, J.L. Cognitive and neuropsychiatric correlates of EEG dynamic complexity in patients with Alzheimer's disease. *Prog. Neuropsychopharmacol. Biol. Psychiatry* **2013**, *47*, 52–61.

27. Richman, J.S.; Moorman, J.R. Physiological time-series analysis using approximate entropy and sample entropy. *Am. J. Physiol. Heart Circ. Physiol.* **2000**, *278*, H2039–H2049.

28. Van Veen, B.D.; van Drongelen, W.; Yuchtman, M.; Suzuki, A. Localization of brain electrical activity via linearly constrained minimum variance spatial filtering. *IEEE Trans. Biomed. Eng.* **1997**, *44*, 867–880.

29. Oostenveld, R.; Fries, P.; Maris, E.; Schoffelen, J.M. FieldTrip: Open source software for advanced analysis of MEG, EEG, and invasive electrophysiological data. *Comput. Intell. Neurosci.* **2011**, *2011*, doi:10.1155/2011/156869.

30. Maris, E.; Oostenveld, R. Nonparametric statistical testing of EEG- and MEG-data. *J. Neurosci. Methods* **2007**, *164*, 177–190.

31. Groppe, D.M.; Urbach, T.P.; Kutas, M. Mass univariate analysis of event-related brain potentials/fields II: Simulation studies. *Psychophysiology* **2011**, *48*, 1726–1737.

32. Benjamini, Y.; Hochberg, Y. Controlling the False Discovery Rate—A Practical and Powerful Approach to Multiple Testing. *J. R. Stat. Soc. Ser. B* **1995**, *57*, 289–300.

33. Verbruggen, F.; Aron, A.R.; Stevens, M.A.; Chambers, C.D. Theta burst stimulation dissociates attention and action updating in human inferior frontal cortex. *Proc. Natl. Acad. Sci. USA* **2010**, *107*, 13966–13971.

34. Duann, J.R.; Ide, J.S.; Luo, X.; Li, C.S. Functional connectivity delineates distinct roles of the inferior frontal cortex and presupplementary motor area in stop signal inhibition. *J. Neurosci.* **2009**, *29*, 10171–10179.

35. Takahashi, T.; Cho, R.Y.; Murata, T.; Mizuno, T.; Kikuchi, M.; Mizukami, K.; Kosaka, H.; Takahashi, K.; Wada, Y. Age-related variation in EEG complexity to photic stimulation: A multiscale entropy analysis. *Clin. Neurophysiol.* **2009**, *120*, 476–483.

36. Anne, H.H. The Multiscale Entropy Algorithm and Its Variants: A Review. *Entropy* **2015**, *17*, 3110–3123.

37. Morabito, F.C.; Labate, D.; la Foresta, F.; Bramanti, A.; Morabito, G.; Palamara, I. Multivariate Multi-Scale Permutation Entropy for Complexity Analysis of Alzheimer's Disease EEG. *Entropy* **2012**, *14*, 1186–1202.

38. Ahmed, M.U.; Mandic, D.P. Multivariate Multiscale Entropy Analysis. *IEEE Signal Process. Lett.* **2012**, *19*, 91–94.

39. Mandic, D.P.; Rehman, N.U.; Wu, Z.; Huang, N.E. Empirical Mode Decomposition-Based Time-Frequency Analysis of Multivariate Signals: The Power of Adaptive Data Analysis. *IEEE Signal Process. Lett.* **2013**, *30*, 74–86.